Accretion-ejection connection in the young brown dwarf candidate ISO-ChaI 217[★]

Whelan, E.T.[1], Alcalá, J.M.[2], Bacciotti, F.[3], Nisini, B.[4], Bonito, R.[5,6], Antoniucci, S.[4], Stelzer, B.[6], Biazzo, K.[2], D'Elia, V.[7], and T.P. Ray.[8]

[1] Institut für Astronomie und Astrophysik, Kepler Center for Astro and Particle Physics, Eberhard Karls Universität, 72076 Tübingen, Germany
[2] INAF-Osservatorio Astronomico di Capodimonte, via Moiariello, 16, I-80131, Napoli, Italy
[3] INAF-Osservatorio Astrofisico di Arcetri, Largo E. Fermi 5, I-50125 Firenze, Italy
[4] INAF-Osservatorio Astronomico di Roma, via Frascati 33, I-00040 Monteporzio Catone, Italy
[5] Dipartimento di Fisica e Chimica, Università di Palermo, Piazza del Parlamento 1, I-90134 Palermo, Italy
[6] INAF-Osservatorio Astronomico di Palermo, Piazza del Parlamento 1, I-90134 Palermo, Italy
[7] ASI Science Data Center, Via del Politecnico snc, I-00133 Rome, Italy
[8] Dublin Institute for Advanced Studies, 31 Fitzwilliam Place, Dublin 2, Ireland

ABSTRACT

As the number of observed brown dwarf outflows is growing it is important to investigate how these outflows compare to the well-studied jets from young stellar objects. A key point of comparison is the relationship between outflow and accretion activity and in particular the ratio between the mass outflow and accretion rates ($\dot{M}_{out}/\dot{M}_{acc}$). The brown dwarf candidate ISO-ChaI 217 was discovered by our group, as part of a spectro-astrometric study of brown dwarfs, to be driving an asymmetric outflow with the blue-shifted lobe having a position angle of ∼ 20°. The aim here is to further investigate the properties of ISO-ChaI 217, the morphology and kinematics of its outflow, and to better constrain $\dot{M}_{out}/\dot{M}_{acc}$. The outflow is spatially resolved in the [S II] $\lambda\lambda 6716, 6731$ lines and is detected out to ∼ 1″.6 in the blue-shifted lobe and 1″ in the red-shifted lobe. The asymmetry between the two lobes is confirmed although the velocity asymmetry is less pronounced with respect to our previous study. Using thirteen different accretion tracers we measure $\log(\dot{M}_{acc})$ [M$_\odot$/yr]= -10.6 ± 0.4. As it was not possible to measure the effect of extinction on the ISO-ChaI 217 outflow $\dot{M}_{out}$ was derived for a range of values of A$_v$, up to a value of A$_v$ = 2.5 mag estimated for the source extinction. The logarithm of the mass outflow ($\dot{M}_{out}$) was estimated in the range -11.7 to -11.1 for both jets combined. Thus $\dot{M}_{out}/\dot{M}_{acc}$ [M$_\odot$/yr] lies below the maximum value predicted by magneto-centrifugal jet launching models. Finally, both model fitting of the Balmer decrements and spectro-astrometric analysis of the Hα line show that the bulk of the H I emission comes from the accretion flow.

Key words. stars: brown dwarfs–jets– Accretion, accretion disks

1. Introduction

Jets and outflows are an integral part of the star formation process and models of jet launching and propagation developed for low mass young stellar objects (YSOs) may also apply to a diverse range of astrophysical objects, including jets driven by brown dwarfs (BDs) (Frank et al., 2014; Joergens et al., 2013). BDs are now routinely observed in star forming regions and therefore it is important to understand how they form and evolve (Luhman, 2012). A key way to do this is to investigate their accretion and outflow properties and compare them to YSOs. Since evidence first emerged that BDs launch outflows (Fernández & Comerón, 2001; Whelan et al., 2005) the number of BD outflows, both atomic and molecular has grown to ∼ 10 (Phan-Bao et al., 2008; Whelan et al., 2012; Joergens et al., 2012; Stelzer et al., 2013; Monin et al., 2013). While this is still a statistically small sample, the comparison between BD outflows and those driven by Class II YSOs i.e classical T Tauri stars (CTTSs) has proven to be very interesting (Whelan et al., 2009b, 2011). Similarities include the observation of a knotty jet which is a signature of episodic accretion (Whelan et al., 2012), the de-

tection of molecular components to known BD optical outflows (Phan-Bao et al., 2008; Monin et al., 2013), the presence of both high and low velocity components to the outflows (Whelan et al., 2009a) and the discovery of an asymmetric BD jet (Whelan et al., 2009b; Joergens et al., 2012).

The high angular resolution observations needed to directly probe the appropriateness of jet launching models developed for YSOs, in the BD mass regime, are not currently possible due to the faintness of the BD outflow emission (Ray et al. , 2007). However, the ratio of the mass outflow to accretion rate ($\dot{M}_{out}/\dot{M}_{acc}$) is constrained by jet launching models and can be investigated in BDs. The first attempts at measuring this ratio in BDs yielded values of $\dot{M}_{out}/\dot{M}_{acc}$ which were significantly higher than the ∼ 10% measured for low mass YSOs and than the predictions made by magneto-centrifugal jet launching models (Whelan et al., 2009b). Magneto-centrifugal jet launching models place an upper limit (per jet) of ∼ 0.3 on this ratio (Ferreira et al. , 2006; Cabrit, 2009). However, as discussed in Whelan et al. (2009b, 2014a), observational biases had a strong influence on these first studies. How this ratio compares in BDs and low mass YSOs could tell us something very important about how BDs form. Therefore, observations specifically designed for measurements of $\dot{M}_{out}/\dot{M}_{acc}$, and of a greater number of BDs are needed.
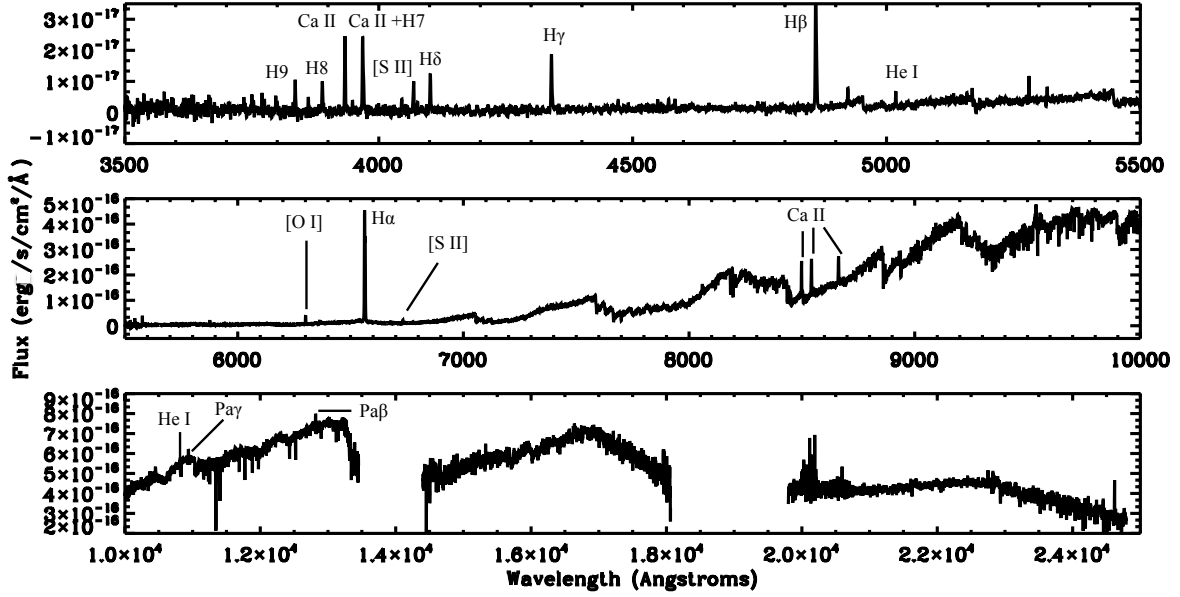

Fig. 1. The full X-Shooter spectrum of ISO-ChaI 217. Key lines are marked and the fluxes of these lines are given in Table 1. Here the spectrum has been smoothed to increase the SNR of key features. The spectra have not been extinction corrected.
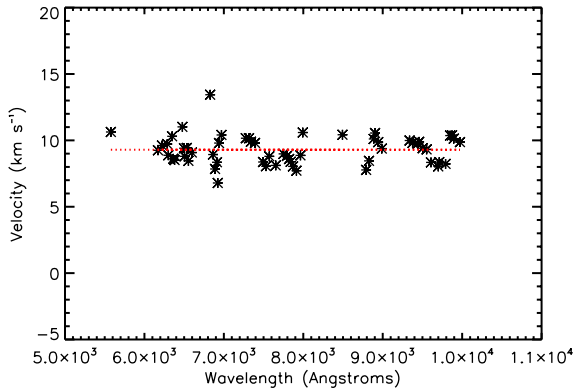

Fig. 2. The velocity of various telluric lines across the wavelength range of the VIS arm of X-Shooter . The difference between the calibration performed by the pipeline and the velocity of the telluric lines is ~ 9 kms^{-1}.

In Whelan et al. (2009b) visible spectra of a sample of BDs at orthogonal slit position angles (PA) was obtained. Spectroastrometry (SA) was used to confirm that the BDs were driving outflows and the orthogonal data allowed the PAs of the outflows to be constrained. As a follow-up to this discovery study, ISO-ChaI 217 the target with the strongest jet emission and most interesting properties, was observed with X-Shooter. The aim of these observations was spatially resolve the ISO-ChaI 217 outflow by placing the slit along the estimated outflow PA and to refine earlier measurements of $\dot{M}_{out}/\dot{M}_{acc}$. Here the results of this X-Shooter study of ISO-ChaI 217, are presented. The full X-Shooter spectrum is shown in Figure 1 and the fluxes of identified lines are given in Table 1. The fundamental parameters of ISO-ChaI 217 are derived and discussed in Section 3.1 and the morphology and kinematics of the jet are discussed in Section 3.3. $\dot{M}_{acc}$ is calculated from the luminosity of various accretion

tracers and $\dot{M}_{out}$ from the luminosity of the [S II] $\lambda 6731$ line, using the approach of Whelan et al. (2014a) (see Section 4.1). Finally, the origin of the permitted emission in the spectrum of ISO-ChaI 217 is investigated through the Balmer decrements (Section 4.2). This work is part of a larger study to investigate the accretion-ejection connection in BDs and very low mass stars (VLMSs) (Whelan et al., 2014a; Giannini et al., 2013; Stelzer et al., 2013)

2. Target, observations and analysis

2.1. Target

ISO-ChaI 217 ($11^h09^m52^s.2$, $-76°39'12."8$) is a young very low mass object located in the Chamaeleon I dark cloud (d∼140 ± 20 pc; Persi et al. 2000). **Its spectral type has been reported as being M6.25 and comparison with models give it a mass of 80 M$_{JUP}$, a radius of 0.64 R$_{\odot}$ and luminosity L$_{bol}$ = 0.023 to 0.028 (Muzerolle et al., 2005; Luhman, 2007).** This mass estimate places it at the hydrogen burning mass limit therefore it is reasonable to describe it as a good candidate for being a young BD. Describing it as a BD candidate is also consistent with previous studies of this object. **Luhman (2007) assign an age of 5-6 Myr to the northern part of the cloud in which ISO-ChaI 217 lies.** Muzerolle et al. (2005) also report log($\dot{M}_{acc}$) = -10 M$_{\odot}$yr^{-1} for ISO-ChaI 217. This estimate of $\dot{M}_{acc}$ is derived by fitting the Hα line profile with magnetospheric accretion models. Note that the authors do not give any error estimate for this value of $\dot{M}_{acc}$. Whelan et al. (2009b, 2014b) measured the PA of the blue-shifted outflow at 20° ± 10° and reported its interesting asymmetry. The asymmetry was revealed in the relative brightness of the two lobes of the outflow (the redshifted lobe was brighter), the difference in the radial velocity of the two (the redshifted lobe was faster) and the difference in the electron density (again higher in the red lobe). Whelan et al. (2009b) also estimated $\dot{M}_{out}/\dot{M}_{acc} > 1$ for ISO-ChaI 217. The results of Whelan

λ_{air} (Å)	Ion	Type	E_u (cm^{-1})	Jet	λ_{obs} (Å)	Flux
		Identification				
3734.4	H I	13 - 2	109029.8		3734.3	0.6 ± 0.5
3750.2	H I	12 - 2	108917.1		3750.1	0.8 ± 0.5
3770.6	H I	11 - 2	108772.3		3770.4	0.7 ± 0.4
3797.9	H I	10 - 2	108582.0		3797.5	1.1 ± 0.4
3835.3	H I	9 - 2	108324.7		3835.4	3.0 ± 0.4
3889.0	H I	8 - 2	107965.1		3888.9	2.7 ± 0.4
3933.7	Ca II	$^2P_{3/2}$-$^2S_{1/2}$	25414.4		3933.5	5.6 ± 0.3
3968.2^a	Ca II	$^2P_{1/2}$-$^2S_{1/2}$	25191.5		3968.2	4.5 ± 0.3
3970.1	H I	7 - 2	107440.5		3969.9	2.1 ± 0.3
4101.7	H I	6 - 2	106632.2		4101.5	2.6 ± 0.3
4340.5	H I	5 - 2	105291.7		4340.2	4.2 ± 0.2
4861.3	H I	4 - 2	102823.9		4860.9	11.2 ± 0.15
5875.9	He I	$^3D_1$-$^3P_0$	186101.7		5876.2	2.9 ± 0.2
6300.3	[O I]	$^1D_1$-$^3P_2$	15867.9	Blue	6300.3	4.25 ± 0.2
				Red	6300.3	4.25 ± 0.2
6363.7	[O I]	$^1D_2$-$^3P_1$	15867.9		6363.7	2.6 ± 0.2
6562.8	H I	3 - 2	97492.3		6563.1	195.0 ± 0.2
6583.5	[N II]	$^1D_2$-$^3P_2$	15316.2	Blue	6583.3	1.2 ± 0.2
6678.2	He I	$^1D_2$-$^1P_1$	186105.1		6678.8	1.5 ± 0.2
6716.4	[S II]	$^2D_{5/2}$-$^4S_{3/2}$	14884.7	Blue	6716.4	1.1 ± 0.2
				Red	6717.7	1.25 ± 0.2
6730.8	[S II]	$^2D_{3/2}$-$^4S_{3/2}$	14852.9	Blue	6731.7	1.8 ± 0.2
				Red	6732.0	2.2 ± 0.2
7065.2	He I	$^3S_1$-$^3P_0$	183236.9		7065.8	1.0 ± 0.2
7172.0	[Fe II]	$a^2G_{7/2}$-$a^4F_{7/2}$	16369.4		7172.4	0.8 ± 0.2
7432.3	[Fe II]	$b^2F_{5/2}$-$a^2P_{3/2}$	31811.82		7432.9	1.5 ± 0.2
8498.0	Ca II	$^2P_{3/2}$-$^2D_{3/2}$	25414.4		8498.6	25.8 ± 0.2
8542.1	Ca II	$^2P_{3/2}$-$^2D_{5/2}$	25414.4		8542.5	38.4 ± 0.2
8662.1	Ca II	$^2P_{1/2}$-$^2D_{3/2}$	25191.5		8662.5	30.2 ± 0.2
10938.0	H I	0 - 3	106632.2		10937.9	33.2 ± 0.3
12818.1	H I	5 - 3	105291.7		12817.7	56.5 ± 0.5

Table 1. Emission Lines identified in the spectrum of ISO-ChaI 217 . Fluxes are in units of erg/s/cm$^2 \times 10^{-17}$ and are not corrected for extinction. $^{(a)}$ blended lines.

et al. (2009b) were upheld by a subsequent investigation of the properties of ISO-ChaI 217 by Joergens et al. (2012). Moreover, Joergens et al. (2012) investigated the properties of the disk of ISO-ChaI 217 inferring a disk inclination angle of $\sim 45°$ and a disk mass of 4×10^{-6} M$_\odot$. Todorov et al. (2014) report the possible detection of a companion to ISO-ChaI 217 (ISO-ChaI 217 B) with a binary separation of ~ 5 AU and a PA of $238° \pm 8°$. The presence of a companion which is interacting with the disk of the jet source could explain the observed asymmetry between the lobes of the jet.

2.2. Observations

The X-Shooter observations presented in this paper were conducted on April 17 2012, on the VLT as part of the INAF X-Shooter GTO program on star forming regions (Alcalá et al., 2011). The single-node exposure time was 850 sec, yielding a nominal exposure time of almost 2 hours after 2 (ABBA) cycles. The average seeing was 0.′′8 during the observations. The slit was aligned with the jet axis and the slit widths of the UVB, VIS and NIR arms were 1.′′0, 0.′′9 and 0.′′9 respectively. This choice of slit widths yielded spectral resolutions of 5100, 8800 and 5600 for each arm, respectively. The pixel scale is 0.′′16 for the UVB and VIS arms and 0.′′21 for the NIR arm. More details of the obser-

vations of the GTO program can be found in Alcalá et al. (2011) and Alcalá et al. (2014).

2.3. Data analysis

The X-Shooter data reduction was performed independently for each arm using the X-Shooter pipeline version 1.3.7. The pipeline provides 2-dimensional, bias-subtracted, flat-field corrected, order-merged, background-subtracted and wavelength-calibrated spectra, but special attention was given to the sky subtraction. Sky regions free of nebular emission were selected along the slit to derive a sky spectrum which was then subtracted to the 1-dimensional spectrum. Flux calibration was achieved within the pipeline using a response function derived from the spectra of flux-calibrated standard stars observed on the same night and of ISO-ChaI 217. Following the independent flux calibration of the X-Shooter arms, the internal consistency of the calibration was checked by plotting together the three spectra extracted from the source position and visually examining the superposition of overlapping spectral regions at the edge of each arm. The UVB and VIS arms were found to be very well aligned, while the NIR arm presented a shift with respect to the VIS spectrum of $\sim 25\%$ lower. This was corrected for by scaling the NIR spectrum to the VIS continuum level. Finally, the correction
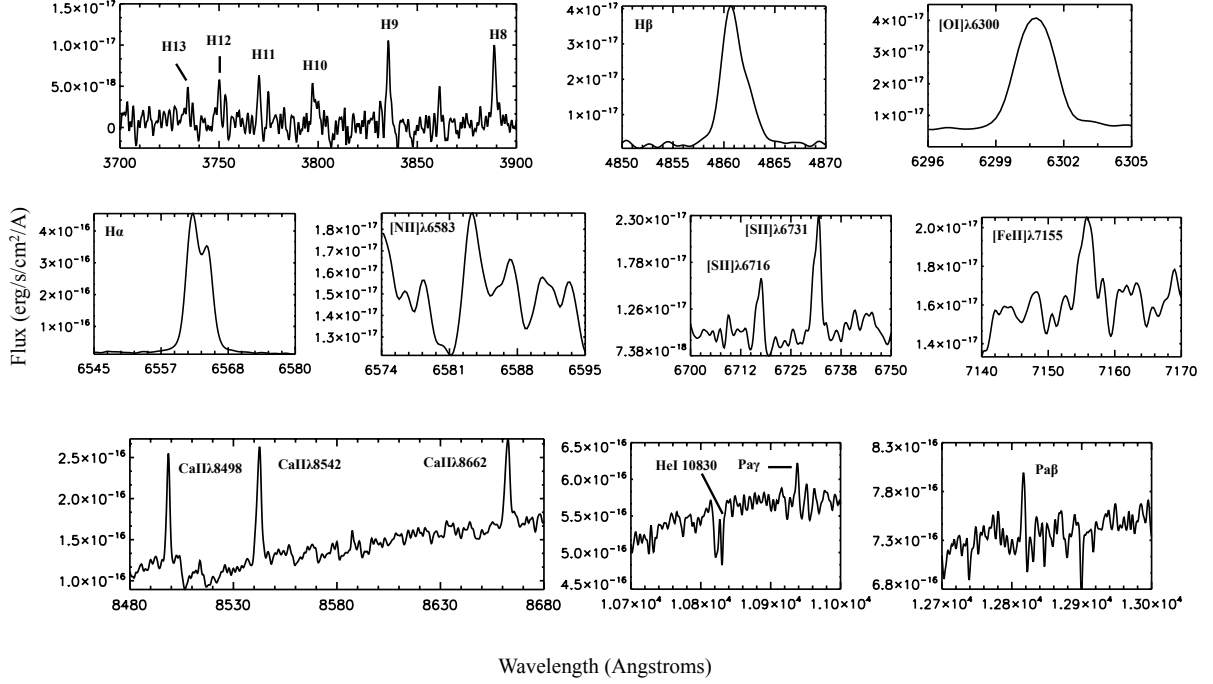
Fig. 4. Spectrum as shown in Figure 1 with a zoom on key accretion and outflow tracers.
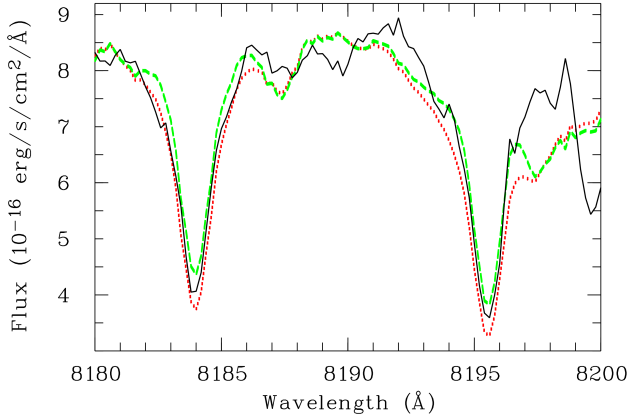

Fig. 3. Detail of the X-shooter spectrum of ISO Cha I-217 (black solid line) in the wavelength range around the Na I $\lambda\lambda$ 8183.3, 8194.8 Å absorption doublet. The spectrum of ISO-ChaI 217 has been corrected for extinction and for telluric absorption lines. The green and the red dotted lines represent synthetic spectra with $\log g$ values of 3.5 and 4.0, respectively, for T_{eff} =2950 K and rotationally broadened to $v \sin i$ =20 km s^{-1}.

for the contribution of telluric bands was done using the telluric standards observed with the same instrumental set-up, and close in airmass to ISO-ChaI 217. More details on data reduction, as well as on flux calibration and correction for telluric bands can be found in Alcalá et al. (2014).

The absolute velocity calibration provided by the X-Shooter pipeline was checked using the OH telluric lines distributed across the wavelength range of X-Shooter. We found an average difference of ~ 9 km s^{-1} between the calibration performed by the pipeline and that done using the telluric lines. In Figure 2 the measured velocities of the telluric lines over the wavelength

range in which the outflow is detected is shown. The spectra were corrected for this velocity difference. All velocities given in this paper are also corrected for the stellar rest velocity of ISO-ChaI 217 measured with respect to the local standard of rest (LSR). In Whelan et al. (2009b) the average velocity of YSOs in Cha I of 2 km s^{-1} was adopted for the stellar rest velocity of ISO-ChaI 217. Joergens et al. (2012) measured the rest velocity of ISO-ChaI 217 to be ~6.6 km s^{-1}, from the Li I absorption feature at ~ 6708 Å. Here we adopt the value to be ~ 6.4 km s^{-1} as measured from the same Li I feature. For the position-velocity (PV) diagrams presented here, both the continuum emission and any sky lines were removed. This was done using the *continuum* routine within the Image Reduction and Analysis Facility (IRAF)[1]. Each continuum row or background column was plotted separately, the extent of the continuum or sky line fitted and then the fit was subtracted. For Figures 1, 4 and 5 Gaussian smoothing was used to increase the signal to noise ratio (SNR). This is commonly done in studies of BD outflows (Whelan et al., 2007, 2009b).

3. Results

3.1. Fundamental parameters of ISO-ChaI 217

The spectral type M6.5 (±0.5) we assign to ISO-ChaI 217 was derived as the average spectral type resulting from the various indices calculated from the VIS spectrum and following Riddick et al. (2007). It is in agreement with determinations in the literature (see Section 2.1), and according to the scale by Luhman et al. (2003) the corresponding temperature is T_{eff} =2940 K, is also in agreement with previous determinations. In Luhman

---

[1] IRAF is distributed by the National Optical Astronomy Observatory, which is operated by the Association of the Universities for Research in astronomy. inc. (AURA) under cooperative agreement with the National Science Fundation
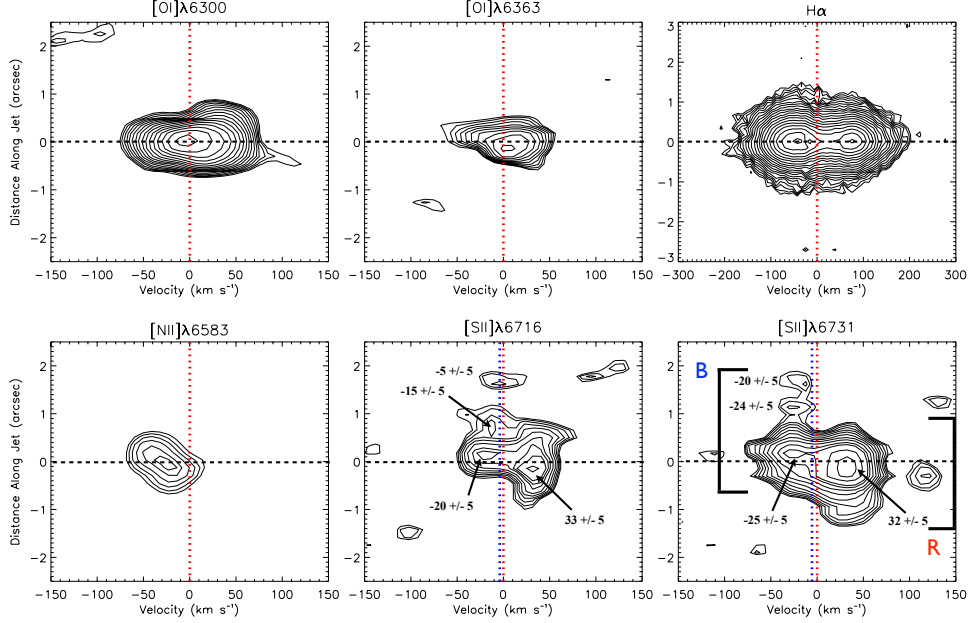
Fig. 5. Contour plots for the main emission lines. Velocities are with respect to the systemic velocity of the source. The zero spatial position is the centre of the continuum emission, measured using Gaussian fitting, and is taken to be the source position. For the [O I] $\lambda\lambda6300, 6363$ and Hα lines, contours start at 3σ and for the [N II] $\lambda6583$ and [S II] $\lambda\lambda6716, 6731$ lines they start at 2σ. The 1σ value is 1×10^{-18} erg/s/cm^2. This is done to highlight the presence of faint extended blue-shifted [SII] emission and the non-detection of even fainter red-shifted [NII]$\lambda6583$ emission. In all cases, contours increase with a log scale ($\sqrt{1.5}$ for the [NII] and [SII] lines). The blue dashed lines mark the velocity of the faint [SII]$\lambda6716, 6731$ background lines.

(2007) an extinction of A_J = 0.68 mag is derived, meaning A_V = 2.1 mag. Here the extinction law by Weingartner & Draine (2001) for R_V=5.5 was used. This law covers a wide range in wavelength, from the UV to the mid-IR. We estimated extinction in the same way as in our previous investigations (Stelzer et al., 2013; Alcalá et al., 2014; Whelan et al., 2014a), that is, by finding the best match of artificially reddened X-shooter spectra of zero-extinction Class III templates, with the spectrum of ISO-ChaI 217. We derived A_V = 2.5 ± 0.3 mag, in fairly good agreement with the value reported by Luhman et al. (2003).

Both mass and radius are crucial physical parameters for the estimates of the mass accretion rate (see Section 4.1). The values derived by Muzerolle et al. (2005) by comparison with the evolutionary models by Baraffe et al. (1998) and Chabrier et al. (2000) are consistent with an object at the hydrogen burning limit. Another check for the temperature and radius can be done by determining the surface gravity, log g, using spectral diagnostics and synthetic spectra. In order to estimate the surface gravity, log g, and as a by-product the projected rotational velocity, $v \sin i$, we used the gravity- and temperature-sensitive absorption doublets of Na I at $\lambda\lambda$ 8183.3, 8194.8 nm and of K I at $\lambda\lambda$ 7664.8, 7698.9 nm, by comparing the X-Shooter data to synthetic spectra. The BT-Settl model spectra of Allard et al. (2011) were used for a range of T_{eff} around the expected value and a range of log g values. The synthetic spectra were binned to the same spectral resolution as the X-Shooter data, and rotationally broadened in steps of $v \sin i$ of 5 km s^{-1} in the range from 10 to 35 km s^{-1}. As an example, the synthetic spectra for T_{eff}=2950 K with two different values of log g are overlaid in Fig. 3 on the X-shooter spectrum of ISO-ChaI 217 in the region of the Na I doublet. The model spectra have been rotationally broadened to $v \sin i$ =20 km s^{-1}, the rotation rate at which the models best

fit the observed spectrum. The width of the observed lines is in agreement with a log g between 3.5 and 4.0. Thus, the parameters for ISO-ChaI 217, T_{eff} =2950 K, log g =3.7(±0.3) and $v \sin i$ =20(±5) km s^{-1} provide the best fit to the data, with the uncertainties being due to the adopted steps in both log g and $v \sin i$ in the grid of synthetic spectra. The gravity derived from the spectrum is in perfect agreement with the value calculated from the mass and radius as derived by Muzerolle et al. (2005) from evolutionary models. **As a consequence, we confirm the results on luminosity and age reported in Muzerolle et al. (2005) and Luhman (2007) (also see Section 2.1.)**

3.2. Line identification

The full UVB, VIS and NIR spectra of ISO-ChaI 217 are presented in Figure 1. By placing the X-Shooter slit along the outflow PA and using the nodding mode the outflow emission is traced to 8 ″ on either side of the driving source. The plotted 1D spectra were extracted by summing over the whole spatial extent of the 2D spectra and thus all the outflow emission is included. The only resolved emission along the slit is in the [S II] $\lambda\lambda6716, 6731$ lines and therefore there is no contribution from extended emission in any of the other lines. The identified lines are marked in Figure 1. Emission lines were identified using the Atomic Line List database (http://www.pa.uky.edu/~peter/atomic/). For the identification, we considered a wavelength uncertainty of about 0.5 Å. Nebular lines from abundant species having excitation energies below 40,000 cm^{-1} were searched for. Line fluxes were computed through the Gaussian fitting of the line profiles after subtraction of the local continuum. Gaussian fitting was done using the

IRAF task *splot*. Absolute flux errors were computed from the root mean square (r.m.s) noise (measured in a portion of the spectrum adjacent to the line) multiplied by the spectral resolution element at the considered wavelength. The line fluxes are not corrected for extinction and a discussion on estimating the on-source extinction of ISO-ChaI 217 is given in Section 3.1. The spatial range over which the flux of the [S II] $\lambda\lambda6716, 6731$ was measured is marked in Figure 5. The same range is used for the [N II] $\lambda6583$ emission and only blue-shifted emission is detected. In the case of the [O I] $\lambda6300$ line it is assumed that total flux is divided evenly between the two outflow lobes. For the other lines listed in Table 1 fluxes are measured from the 1D spectrum.

In Figure 4 line profiles of some of the most interesting lines are plotted. Firstly note that the Balmer lines from H13 to Hα are detected. In Section 4.2 these lines are used to compute the Balmer decrements with respect to the Hβ line. The Hα line has a shape typical of an accretion dominated Hα line region. While the outflow is not resolved in velocity in the [O I] $\lambda6300$ line the [S II] $\lambda\lambda6716, 6731$ line regions are double peaked (especially clear in the unsmoothed data) with the red-shifted peak being brighter. Thus we can extract velocity information from these lines and the X-Shooter line profile compares well to what was reported in Whelan et al. (2009b), in that the line is double peaked and the red-shifted peak is brighter. We discuss the [S II] $\lambda\lambda6716, 6731$ line regions further in Section 3.3. The CaII triplet, a further strong indicator of accretion is also detected. The HeI 1.083 μm line is seen in blue-shifted absorption. Finally the Paγ and Paβ lines while faint are detected and are used in Section 4.1 to estimate $\dot{M}_{acc}$.

3.3. Kinematics and morphology of the ISO-ChaI 217 jet

In Whelan et al. (2009b) it was demonstrated using SA that the [O I] $\lambda\lambda6300, 6363$ and [S II] $\lambda\lambda6716, 6731$ lines were formed in the outflow of ISO-ChaI 217. As the spectra presented here were taken with the slit aligned parallel to the estimated outflow PA, it is now possible to investigate the kinematics and morphology of this outflow along the jet axis. In Figure 5 PV diagrams of the brightest outflow lines plus Hα are presented. **The Hα line is the only line included in this figure that traces both outflow accretion as the FELs are quenched at the densities of the accretion shocks (Hirth et al., 1997).** Our discussion of the kinematics and morphology of the outflow is based on this Figure. Firstly, from Figure 5 it is clear that the outflow is spatially resolved in the [S II] $\lambda\lambda6716, 6731$ lines. This confirms that the estimate of the outflow PA derived by Whelan et al. (2009b) was accurate. The blue-shifted lobe extends to ~ 1.6 '' and the red-shifted lobe to ~ 1 ''. As described in Section 2 the velocity is measured with respect to the stellar rest velocity of ISO-ChaI 217. In Figure 5 the velocities for the different components seen in the outflow are given. The red-shifted flow is marginally faster than the blue-shifted flow. Thus the velocity asymmetry reported in Whelan et al. (2009b) and Joergens et al. (2012) is not as pronounced in this dataset. For example, Whelan et al. (2009b) gave the velocities of the blue and red-shifted lobes at -20 km s^{-1} and -40 km s^{-1} respectively. Therefore, in that study the ratio of velocity between the red and blue lobes is 2.0 as compared to the value of 1.4 found here. The difference between these two sets of velocities is due to the different values for the stellar rest velocity adopted (see Section 2) and also likely due to the fact that in Whelan et al. (2009b) we were not observing along the outflow. Overall the radial velocities measured here can be considered to be more accurate.

As well as the small velocity asymmetry between the two lobes there is also a clear morphological asymmetry. The blue-shifted lobe has three separate knots while only one knot is resolved in the red-shifted lobe. Although the blue-shifted emission at ~ 1 '' and ~ 1.6 '' is faint we are satisfied that the fact that it is seen in both [SII] lines rules out the possibility that this is noise. We also consider the fact that the extended emission is due to an imperfect subtraction of faint background [S II] $\lambda\lambda6716, 6731$ emission. These background lines are a signature of nebular emission surrounding ISO-ChaI 217 and the velocity at which we see these lines is marked in Figure 5 by the blue dashed lines. For the [S II] $\lambda6716$ and [S II] $\lambda6731$ knots at ~ 1 '' there is enough of a separation in velocity from the background lines for us to conclude that these knots are real. Also the same argument applies for the [S II] $\lambda6731$ knot at ~ 1.6 ''. The [S II] $\lambda6716$ emission at 1.6 '' does lie at the velocity of the background line. Thus, we cannot categorically say without higher SNR data, that this is a knot in the outflow. However, the fact that its position coincides with a [S II] $\lambda6731$ knot and the fact that we see no such extended emission in the other jet lines after sky subtraction makes it likely that it is a knot. By comparing the radial velocities of three [SII] knots in the blue-shifted outflow, it is seen that there is a small decrease in radial velocity along the blue-shifted flow. A decrease in velocity with distance is often seen in jets from YSOs (Davis et al., 2003). This can be explained by numerical simulations which show that speed of the shock front is lower than the initial velocity of ejection, due to the interaction with the ambient medium which decelerates the outflow (Bonito et al., 2004, 2007).

From Figure 5 it can also be seen that the outflow is not spatially resolved in the [O I] $\lambda\lambda6300, 6363$ lines. This is not surprising as the critical density of the [OI] lines is two orders of magnitude higher than the critical density of the [SII] lines. Therefore [OI] forms closer to the driving source of the outflow than the [SII] which often traces more extended emission (Hartigan et al., 1995). This difference between the spatial extent of the [O I] $\lambda\lambda6300, 6363$ and [S II] $\lambda\lambda6716, 6731$ lines was also noted by Whelan et al. (2009b). Whelan et al. (2009b) measured offsets of ~ 200 mas in the [SII] lines while the [OI] were only extended to ~ 50 mas. In Figure 6 the results of applying SA to the X-Shooter [O I] $\lambda6300$ line region are presented. This analysis confirms that the [OI] emission detected in the X-Shooter spectrum is formed in the ISO-ChaI 217 outflow, and the offsets are larger than those measured in Whelan et al. (2009b) as expected for a spectrum taken along the outflow PA. In Figure 6 the spectro-astrometric analysis of the Hα line is also shown. We detect no outflow component to the Hα line.

Finally, and very interestingly, it can be seen from Figure 5 that [N II] $\lambda6583$ is only detected in the blue-shifted flow and that it traces slightly higher velocities than the [S II] $\lambda\lambda6716, 6731$ lines. The estimated flux of the [N II] $\lambda6583$ emission is 1.2 $\pm$ 0.2 $\times$ 10^{-17} erg/s/cm^2. The critical density of the blue-shifted [N II] $\lambda6583$ emission is $\sim 6 \times 10^4$ cm^{-3} at 10,000 K and it only traces the highest velocity emission in YSO jets (Hirth et al., 1997). The non-detection of [N II] $\lambda6583$ in the red-shifted flow implies that the ionisation fraction is smaller in the red-shifted lobe than in the blue-shifted lobe (see Table 2). **There are many examples of CTT jets where [N II] $\lambda6583$ is only weakly detected compared to other FELs and thus a low ionisation is inferred. For example (Coffey et al., 2008) discuss the weak [N II] $\lambda6583$ emission from and thus low ionisation of the RW Aur red-shifted jet. Furthermore, better angular resolution observations are needed before one can conclude if partial obscuration by the ISO-ChaI 217 disk could also contribute**
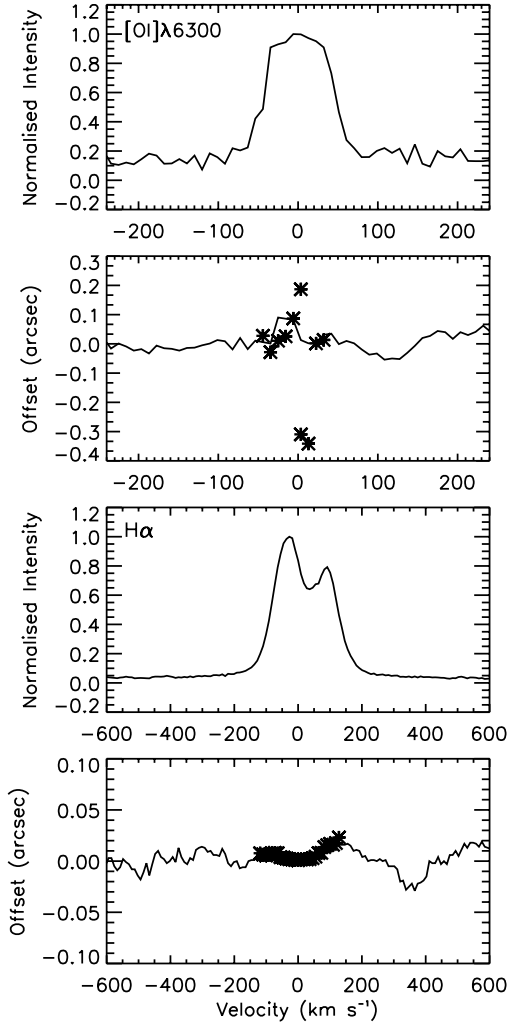
Fig. 6. Spectro-astrometric analysis of the [O I] $\lambda6300$ and Hα lines. Offsets are measured using Gaussian fitting. The black asteriks are the offsets measured after continuum subtraction. The accuracy in the measurement of the offsets is $\sim$ 20 mas. This analysis confims that the [O I] $\lambda6300$ line is tracing the outflow while no outflow component is detected in the Hα line.

to the lack of [N II] $\lambda6583$ emission from the ISO-ChaI 217 red-shifted jet.

4. Discussion

4.1. Estimating $\dot{M}_{out}/\dot{M}_{acc}$

The mass accretion rate was calculated from the following equation

$$\dot{M}_{acc} = 1.25(L_{acc}R_*)/(GM_*) \tag{1}$$

where L_{acc} is the accretion luminosity and R_* and M_* are the stellar radius and mass (Gullbring et al., 1998; Hartmann et al., 1998). L_{acc} is derived from the luminosity of 13 accretion tracers (L_{line}; Figure 8) using the relationships published in Alcalá et al. (2014). L_{line} was calculated from the extinction corrected fluxes (see section 3.1) of the accretion indicators and assuming a distance of 140 pc. **Due to the moderate inclination of the disk (given in Section 2.1) L_{line} did not need to be corrected for obscuration by the disk as in Whelan et al. (2014a).**

Also included is the literature value taken from (Muzerolle et al., 2005). We also consider the effect of variable accretion by comparing log($\dot{M}_{acc}$) derived here from the Hα line to the value derived from the VLT / UVES spectra presented in Whelan et al. (2009b). It can be seen from Figure 7 that these values are compatible within the errors. It is found that the average value for log($\dot{M}_{acc}$) [M$_\odot$/yr]= -10.6 $\pm$ 0.4 which is consistent within errors with the result of (Muzerolle et al., 2005).

In Table 2 the physical parameters of the ISO-ChaI 217 blue and red jets and the derived values of $\dot{M}_{out}$ are given. The physical parameters are the electron density (n_e), the electron temperature (T_e), and the ionisation fraction (x_e). The electron density is estimated from the ratio of the [S II] $\lambda\lambda6716, 6731$, T_e from the ratio [O I] $\lambda6300$/ [S II] $\lambda6731$ and x$_e$ from the ratio [N II] $\lambda6583$ / [O I] $\lambda6300$ (Whelan et al., 2014a). In the case of the ionisation in the red-shifted jet an upper limit of 3 times the r.m.s noise was used for the flux of the [N II] $\lambda6583$ line. The extent to which a YSO jet is extincted by the circumstellar material is an important parameter when calculating $\dot{M}_{out}$ and can be estimated using the [FeII] jet lines at 1.27, 1.32, 1.64μm (Nisini et al., 2005). As these lines are not detected in the spectrum of ISO-ChaI 217 it is not possible to know the level to which the ISO-ChaI 217 jet is extincted by any circumstellar material. Therefore, to test the dependence of the results on the jet extinction, the physical parameters and $\dot{M}_{out}$ were calculated for a range of values of A$_v$ as shown in Table 2. Increasing the extinction and thus the line flux does not substantially effect the values of n$_e$, T_e and x$_e$. It mostly impacts L$_{SII}$ and thus $\dot{M}_{out}$.

The measurements of $\dot{M}_{out}$ are based on the following equations and further information can be found in Whelan et al. (2014a).

$$\dot{M}_{out} = \mu\, m_H\, (n_H\, V)\, V_{tan}/l_t \tag{2}$$

with

$$n_H V = L_{SII} \left(h\,\nu\, A_i\, f_i\, \frac{X^i}{X}\, \frac{X}{H} \right)^{-1} \tag{3}$$

Here μ = 1.24 is the mean atomic weight, m_H the proton mass, V the volume effectively filled by the emitting gas, V_{tan} and l_t the tangential velocity and length of the knot, A_i and f_i the radiative rate and upper level population relative to the considered transition and finally $\frac{X^i}{X}$ and $\frac{X}{H}$ are x$_e$ and the relative abundance of the considered species. The ionisation fraction and the upper level population are estimated from the physical parameters given in Table 2. The tangential velocities of the blue and red jets are taken at 25 km s^{-1} and 32 km s^{-1} respectively, and l$_t$ = 1 ″. We do not include the outer blue-shifted knot in our calculation as we should only include knots which are detected in either [OI]$\lambda6300$ or [NII]$\lambda6583$. L$_{SII}$ is the luminosity of the [SII]$\lambda6731$ line and it is assumed in this calculation that all the sulphur is single ionised.

Overall it is concluded from the results presented in Table 2 that $\dot{M}_{out}/\dot{M}_{acc}$ (two-sided) for ISO-ChaI 217 is consistent with magneto-centrifugal jet launching models and studies of CTTSs. This conclusion applies for all chosen values of A$_v$. In Whelan et al. (2009b) $\dot{M}_{out}$ was measured at 1.8 $\times$ 10^{-10} M$_\odot$yr^{-1} and 3.1 $\times$ 10^{-10} M$_\odot$yr^{-1} for the blue-shifted and red-shifted jets respectively and thus $\dot{M}_{out}/\dot{M}_{acc}$ using the value of $\dot{M}_{acc}$ published by Muzerolle et al. (2005) was > 1. In Whelan et al. (2009b) the extinction of the source and the jet was assumed to be the same. The main reason for the difference between the lower and thus more plausible estimate of $\dot{M}_{out}/\dot{M}_{acc}$ made here, and the value published in Whelan et al. (2009b) is that in Whelan et al.
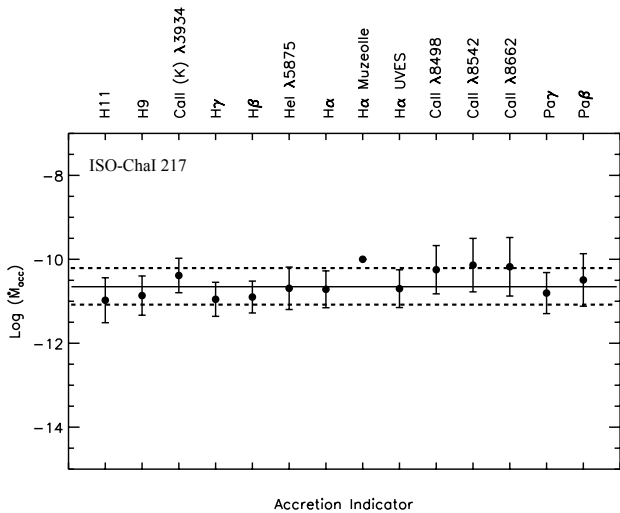
Fig. 7. Mass accretion rate estimated from various accretion tracers. The solid line gives the mean value of log ($\dot{M}_{acc}$) and the dashed line is the $\pm 1\sigma$ uncertainty. The errors on the individual measurements mainly come from the error in the line fluxes and in the value of the on-source extinction. The value of $\dot{M}_{acc}$ calculated by Muzerolle et al. (2005) from modelling of the Hα line and from the UVES spectra presented by Whelan et al. (2009b) are included here for comparison. No error estimates were given in Muzerolle et al. (2005).

which no outflow component is detected. It is likely that the outflow can be traced by the Hα line but the emission is many times fainter than the accretion component. Note that no Brackett lines and only two Paschen lines are detected.
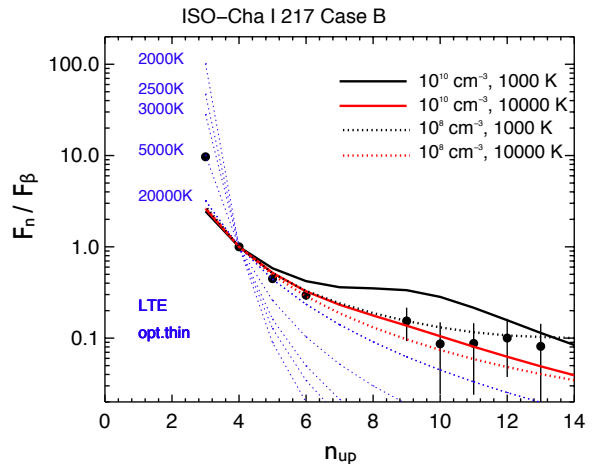

Fig. 8. Balmer decrements. Results seem to be consistent with an accretion scenario, similar to Par-Lup 3-4 .

(2009b) the method used assumed a value for the critical density (n_{cr}) which was highly uncertain. Here an estimate of n_{cr} is not required. Estimates of $\dot{M}_{acc}$ are more accurate due to the use of several accretion tracers. Previous to this work it has only been derived from the Hα line. However, this change in the derived value of $\dot{M}_{acc}$ does not have a significant effect on the final values of $\dot{M}_{out}/\dot{M}_{acc}$. Similarly extinction does not have a large effect on our conclusion in this case. As for all values of A$_v$ up to the value measured for the driving source $\dot{M}_{out}/\dot{M}_{acc}$ remains within the limits of predictions by leading models.

4.2. Investigating the origin of the HI emission

Several HI emission lines are detected in the spectrum of ISO-ChaI 217 (see Figure 4). To investigate the origin of this emission the Balmer decrements were computed with respect to Hβ line and are plotted as a function of upper quantum number (n_{up}) in Figure 8. While the spectral range of X-Shooter covers most of the Balmer lines any lines with $n_{up} > 13$ were found to be too noisy for inclusion in our analysis. Additionally, at the intermediate spectral resolution of X-Shooter the H7 and H8 lines are blended with other lines and are therefore also not included. To constrain the physical conditions in the emitting gas the decrements were firstly compared to standard Case B predictions calculated for a range of temperature and density. The Case B curves were derived using the calculations of Hummer & Storey (1987) and using the Fortran program and data files provided by Storey & Hummer (1995). These models assume that all lines are optically thin. Secondly, the decrements were also compared to optically thick and thin local thermodynamic equilibrium cases (LTE) ratios, calculated over a temperature range of 2000 K to 20000 K. The optically thick case is not shown in Figure 8 as it was not a good fit to the results. The emission is best fit with the Case B model and T_e =10,000 K, n$_e$ = 10^{10} cm^{-3}. This suggests formation in an accretion flow (Martin, 1996). This is consistent with the spectro-astrometric analysis of the Hα line (Figure 6) in

5. Summary

Here we present a follow-up X-Shooter study of the BD candidate ISO-ChaI 217 and its outflow. Previous to this work ISO-ChaI 217 was found to have a bipolar outflow which exhibited various asymmetries and $\dot{M}_{out}/\dot{M}_{acc}$ had been estimated to be > 1. The advantage of using X-Shooter is that the source and outflow can be probed at wavelengths previously not investigated and that $\dot{M}_{acc}$ and $\dot{M}_{out}/\dot{M}_{acc}$ can be more accurately estimated. An additional advantage of this study is that data were collected with the slit aligned with the derived outflow PA thus allowing the technique for estimating the PA of outflows using SA to be tested (Whelan et al., 2009b) and, the morphology and kinematics of the ISO-ChaI 217 jet studied with distance along the jet. The results can be summarised as follows.

- The outflow is spatially resolved in the [SII]$\lambda\lambda$6716, 6731 lines and three separate knots at ~ 0.″1, 0.″7 and 1.″6 are detected in the blue-shifted flow. Red-shifted emission extends to ~ 1 ″ with an emission peak at 0.″2.
- While the velocity asymmetry between the blue-shifted and red-shifted lobes of the outflow is not as pronounced as reported in Whelan et al. (2009b) the red-shifted flow is still found to be faster than the blue-shifted flow. In Whelan et al. (2009b) the factor by which it was faster was ~ 2 while here it is ~ 1.4. There are also morphological asymmetries in that three knots are detected in the blue-shifted jet while only one red-shifted knot is detected. These kinematical and morphological asymmetries can be explained by a pulsed jet model which describes how if different ejection rates are involved in the opposite sides of a bipolar jet, different knot velocities are expected (Bonito et al., 2010a,b). Also $\dot{M}_{out}$ is larger in the red-shifted jet than in the blue-shifted, even when we account for the uncertainty introduced by the use of an upper limit for the flux of the [N II] λ6583 line in the red-shifted jet. This difference in $\dot{M}_{out}$ was also found in Whelan et al. (2009b) and this sort of of asymmetry can be reproduced by

A_v (mag)	0.0	1.0	2.5
n_e Blue (cm^{-3})	4610	4700	4920
n_e Red (cm^{-3})	5490	5630	5750
T_e Blue (10^4 K)	2.15	2.24	2.34
T_e Red (10^4 K)	1.63	1.71	1.81
x_e Blue	0.078	0.063	0.048
x_e Red	0.045	0.040	0.034
n_H Blue (10^4 cm^{-3})	6.0 ± 0.8	7.5 ± 1.0	10.3 ± 1.4
n_H Red (10^4 cm^{-3})	12.2 ± 4.4	14.0 ± 5.0	17.0 ± 6.2
Method B			
L_{SII} Blue (10^{-8} L$_\odot$)	1.1 ± 0.3	2.3 ± 0.4	5.6 ± 1.0
L_{SII} Red (10^{-8} L$_\odot$)	1.4 ± 0.3	2.8 ± 0.5	6.9 ± 1.2
$\dot{M}_{out}$ (10^{-12} M$_\odot$yr^{-1}) Blue	0.7 ± 0.2	1.4 ± 0.3	3.3 ± 0.7
$\dot{M}_{out}$ (10^{-12} M$_\odot$yr^{-1}) Red	1.2 ± 0.5	2.3 ± 0.9	5.3 ± 2.1
($\dot{M}_{out}$ Blue + $\dot{M}_{out}$ Red) / $\dot{M}_{acc}$	0.05 (+0.07)(-0.02)	0.09 (+0.14)(-0.04)	0.20 (+0.30)(-0.09)

Table 2. The jet physical parameters and $\dot{M}_{out}$ for the ISO-ChaI 217 blue and red jets. A_v here refers to the extinction of the jet and the calculations are made for three values of A_v to investigate the dependence on the jet extinction. The mean value of $\dot{M}_{acc}$ ($\dot{M}_{acc}$ mean = 4×10^{-11} M$_\odot$yr^{-1}) is used to calculate $\dot{M}_{out}/\dot{M}_{acc}$ and $\dot{M}_{acc}$ is derived from the fluxes of the accretion tracers listed in Figure 8 corrected for an on-source extinction 2.5 ± 0.3 mag.

the lastest models which account for jet asymmetries (Fendt & Sheikhnezami, 2013).

– Using the improved method for estimate $\dot{M}_{out}$ we now place $\dot{M}_{out}/\dot{M}_{acc}$ (for the ISO-ChaI 217 jets combined) at 0.05 (+0.07)(-0.02). This value assumes that the outflow is not affected by extinction and unlike previous estimates this ratio is now in agreement with predictions of jet launching models (Ferreira et al. , 2006). This agreement still persists even if we assume that the extinction affecting the outflow is comparable to the value of A_v measured here for the source. This is significant as it is one of the few studies which show this ratio to be the same in BDs as in CTTS (Stelzer et al., 2013; Whelan et al., 2014a).

– Finally by analysing the Balmer decrements of the selection of Balmer lines found in the ISO-ChaI 217 spectrum it is concluded that the emission is best fit with a temperature of 10,000 K and a density of 10^{10} cm^{-3}. This confirms that the bulk of the Balmer emission comes from the accretion flow in agreement with the spectro-astrometric analysis of the Hα line.

Overall this work adds to the similarities already observed between BD and CTT outflows. Now as well as having kinematical and morphological properties which are comparable to CTT jets $\dot{M}_{out}/\dot{M}_{acc}$ is also comparable in a few cases. Additionally, it demonstrates the usefulness of SA for determining basic information about a BD outflow such as the outflow PA, and the value of following up such spectro-astrometric investigations with high quality spectroscopic observations made parallel to the jet axis. The methods used here should be applied to a larger number of BD outflows to better constrain $\dot{M}_{out}/\dot{M}_{acc}$ at the lowest masses.

References

Alcalá, J. M., Stelzer, B., Covino, E., et al. 2011, Astronomische Nachrichten, 332, 242
Alcalá, J. M., Natta, A., Manara, C. F., et al. 2014, A&A, 561, A2
Allard, F., Homeier, D., & Freytag, B. 2011, 16th Cambridge Workshop on Cool Stars, Stellar Systems, and the Sun, 448, 91
Baraffe, I., Chabrier, G., Allard, F., et al. 1998, A&A, 337, 403
Bonito, R., Orlando, S., Peres, G., Favata, F., & Rosner, R. 2004, A&A, 424, L1
Bonito, R., Orlando, S., Peres, G., Favata, F., & Rosner, R. 2007, A&A, 462, 645
Bonito, R., Orlando, S., Peres, G., et al. 2010a, A&A, 511, A42
Bonito, R., Orlando, S., Miceli, M., et al. 2010b, A&A, 517, A68
Cabrit, S. 2009, in Protostellar Jets in Context , by Kanaris Tsinganos, Tom Ray, Matthias Stute. Astrophysics and Space Science Proceedings Series, Berlin, Springer p. 247
Chabrier, G., Baraffe, I., Allard, F., & Hauschildt, P. 2000, ApJ, 542, 464
Coffey, D., Bacciotti, F., & Podio, L. 2008, ApJ, 689, 1112
Comerón, F., Fernández, M., Baraffe, I., Neuhäuser, R., & Kaas, A. A. 2003, A&A, 406, 1001
Davis, C. J., Whelan, E., Ray, T. P., & Chrysostomou, A. 2003, A&A, 397, 693
Fendt, C., & Sheikhnezami, S. 2013, ApJ, 774, 12
Ferreira, J.; Dougados, C.; Cabrit. S. 2006 A&A, 453, 785
Fernández, M., & Comerón, F. 2001, A&A, 380, 264
Frank, A., Ray, T. P., Cabrit, S., et al. 2014, arXiv:1402.3553
Giannini, T., Nisini, B., Antoniucci, S., et al. 2013, ApJ, 778, 71
Gullbring, E., Hartmann, L., Briceno, C., & Calvet, N. 1998, ApJ, 492, 323
Hartigan, P., Edwards, S., & Ghandour, L. 1995, ApJ, 452, 736
Hartmann, L., Calvet, N., Gullbring, E., & D'Alessio, P. 1998, ApJ, 495, 385
Hirth, G. A., Mundt, R., & Solf, J. 1997, A&AS, 126, 437
Hummer, D. G., & Storey, P. J. 1987, MNRAS, 224, 801
Joergens, V., Herczeg, G., Liu, Y., et al. 2013, Astronomische Nachrichten, 334, 159
Joergens, V., Pohl, A., Sicilia-Aguilar, A., & Henning, T. 2012, A&A, 543, A151
Luhman, K. L., Stauffer, J., Muench, A., et al. 2003, ApJ, 593, 1093
Luhman, K. L. 2007, ApJS, 173, 104
Luhman, K. L. 2012, ARA&A, 50, 65
Martin, S. C. 1996, ApJ, 470, 537
Monin, J.-L., Whelan, E. T., Lefloch, B., Dougados, C., & Alves de Oliveira, C. 2013, A&A, 551, L1
Muzerolle, J., Luhman, K. L., Briceño, C., Hartmann, L., & Calvet, N. 2005, ApJ, 625, 906
Nisini, B., Bacciotti, F., Giannini, T., et al. 2005, A&A, 441, 159
Persi, P., et al. 2000, A&A, 357, 219
Phan-Bao, N., et al. 2008, ApJ, 689, L141
Ray, T., Dougados, C., Bacciotti, F., Eislöffel, J., & Chrysostomou, A. 2007, Protostars and Planets V, p. 231
Riddick, F., Roche, P., & Lucas, P. 2007, MNRAS, 381, 1067
Stelzer, B., Alcalá, J. M., Scholz, A., et al. 2013, A&A, 551, A106
Storey, P. J., & Hummer, D. G. 1995, VizieR Online Data Catalog, 6064, 0
Todorov, K. O., Luhman, K. L., Konopacky, Q. M., et al. 2014, arXiv:1404.0213
Weingartner, J. C., & Draine, B. T. 2001, ApJ, 548, 296

Whelan, E. T., Ray, T. P., Bacciotti, F., et al. 2005, Nature, 435, 652

Whelan, E. T., Ray, T. P., Randich, S., et al. 2007, ApJ, 659, L45

Whelan, E. T., Ray, T. P., & Bacciotti, F. 2009a, ApJ, 691, L106

Whelan, E. T., Ray, T. P., Podio, L., Bacciotti, F., & Randich, S. 2009b, ApJ, 706, 1054

Whelan, E. T., et al. 2010, ApJ, 720, L119

Whelan, E. T., Bacciotti, F., Ray, T., & Dougados, C. 2011, IAU Symposium, 275, 396

Whelan, E. T., Ray, T. P., Comeron, F., Bacciotti, F., & Kavanagh, P. J. 2012, ApJ, 761, 120

Whelan, E. T., Bonito, R., Antoniucci, S., et al. 2014a, A&A, 565, A80

Whelan, E. T., Ray, T.P., Podio, L., Bacciotti, F., Randich, S. 2014, erratum submitted